Cell Deformation of *Taxodium* Hybrid 'Zhongshanshan' Wood during the Drying Process

Yuehua Zhu,* Xinzhou Wang, Yaoli Zhang, and Biao Pan

Morphological changes were examined in the wood cells of the *Taxodium* hybrid 'zhongshanshan' during the drying process, using wood sectioning and image processing methods. The results showed that the radial and tangential shrinkage rates were 2.7% and 5.8%, respectively. The tracheids displayed greater tangential than radial shrinkages, and latewood tracheids presented greater radial and tangential shrinkages than earlywood tracheids. The wood rays had little effect on cell lumen and tangential shrinkages of tracheids, unless they were adjacent to them. Shrinkage anisotropy was caused by the combined effect of difference between earlywood and latewood, and the inhibitory effect of wood rays. The fiber saturation point of *Taxodium* hybrid 'zhongshanshan' was between 33.3% and 38.3%. This study provided a scientific basis for the drying of the *Taxodium* hybrid 'zhongshanshan'.

Keywords: Taxodium hybrid 'zhongshanshan'; Shrinkage; Drying; Cell; Deformation

*Contact information: College of Materials Science and Engineering, Nanjing Forestry University, Nanjing 210037, China; *Corresponding author: otakuzhu@foxmail.com*

INTRODUCTION

The *Taxodium* hybrid 'zhongshanshan' is an improved tree species obtained by artificial hybridization at the Institute of Botany, Jiangsu Province and Chinese Academy of Sciences. Two species of the genus *Taxodium* (family: Cupressaceae) were chosen for interspecific hybridization experiments. Growing *Taxodium mucronatum* was beneficial for its salt-alkali tolerance, and *Taxodium distichum,* for its rapid growth and good stem form (Shi *et al*. 2016; Hua *et al*. 2017). The *Taxodium* hybrid 'zhongshanshan' shows large deformation, which is not conducive to its development and utilization. Since wood is an irregular, heterogeneous, and anisotropic material (Thuvander *et al*. 2002), the dried wood undergoes deformation during the process of drying due to the various longitudinal, radial, and tangential shrinkages.

Previous studies indicate that both wet and dry wood shows substantial transverse shrinkage while showing small differences on the longitudinal plane. Normally, tangential shrinkage is 1.5 to 2.5 times more than radial shrinkage (Spear and Walker 2006). Understanding the reason of anisotropic shrinkage of wood during drying is critical to the study of wood deformation.

Wood shrinkage generally occurs only when the moisture content (MC) of wood is below the fiber saturation point (FSP) (Panshin and Zeeuw 1980). However, other studies state that wood undergoes elastic deformation when the MC is higher than the FSP, while irreversible plastic deformation occurs when the MC of wood is lower than the FSP (Pambou *et al*. 2017). In addition, wood shrinkage is affected by its anatomical structure, ultrastructure and chemical composition, and the transverse shrinkage of wood is governed mostly by a specific ultrastructural organization of moderately organized cell wall

compounds (Bonarski *et al*. 2015). Therefore, studying the wood microstructure is one of the most important ways to understand the shrinkage rate and deformation of wood.

There are many theories to explain the anisotropic behavior of wood. Among them, the 'ray restraint' theory and 'latewood control' theories are considered the most likely to explain the anisotropy of wood during drying. In the 'ray restraint' theory, wood rays play the vital role in suppressing radial shrinkage because wood ray tissue shrinks less in the radial direction. The results of X-ray computed tomography showed that the shrinkage of cells near the wood ray was less than the shrinkage of cells away from the wood ray, which confirms the 'ray restraint' at the micro-scale (Taylor *et al*. 2013). For the 'latewood control' theory, observation of scots pine indicated that the cell wall of latewood in the radial direction was about 25% thicker than that in the tangential direction, while earlywood did not exhibit this difference (Gu *et al*. 2001). In the process of moisture adsorption and desorption, the average radial changes of latewood was greater than that of earlywood (Dang *et al*. 2018).

However, most of the above-mentioned theories of anisotropic behavior of wood are based on studies in total rather than unit shrinkages. In recent years, there were breakthroughs on single cell deformation research. By combining confocal laser scanning microscope (CLSM) with image processing technologies, changes to cell-end faces in the process of moisture absorption and desorption were clearly observed. In the moisture absorption process of spruce, the tracheids and cell lumen showed tangential linear expansion and irregular radial deformation of the cell lumen. At the micro-level, the cells exhibited a larger tangential than radial expansion (Taguchi *et al*. 2010). In the study of tracheids-expansion of Douglas fir, the MC of the wood was controlled by different saturated salt solutions. The CLSM and digital image correlation method were used to observe the expanding behavior of softwood's latewood. The results showed that the change of the cell lumen was irregular when the MC of wood was close to the saturated vapor pressure and the diameter of the cell lumen presented shrinkage. The cell lumen deformation of the latewood tracheids was more sensitive to changes in ambient temperature and humidity, and it was also affected by cell alignment and the alternation between latewood and earlywood (Murata and Masuda 2006).

The above-mentioned studies determined the morphological changes of single cells during absorption and desorption of MC of wood species. However, in those studies, the MC range was below the FSP, and the cell shape changes in these conditions were not addressed. In this study, wood sectioning and image processing methods were used to determine the morphological changes of the *Taxodium* hybrid 'zhongshanshan' cell during the drying process, and explored the general deformation mechanism of dried *Taxodium* hybrid 'zhongshanshan'. The results from this study will provide a scientific basis for the drying of *Taxodium* hybrid 'zhongshanshan' wood.

EXPERIMENTAL

Specimens

The *Taxodium* hybrid 'zhongshanshan' was obtained from Garden and Seedling Experimental Demonstration Base of the Institute of Botany (Jiangsu Province, China) and Chinese Academy of Sciences (Liuhe District, Nanjing City, Jiangsu Province, China). The average age was 20 years, the average diameter breast height was 30.3cm, and the average wood density was about 324 kg m^{-3} at 12% moisture content. Every sample block was

prepared from mature tree sapwood with dimensions of 20 × 20 × 20 mm, cut with the use of a wheel saw. The sample block was immersed in distilled water for softening, and then cut into 12 slices of 20-μm thickness on the transverse section using a sliding microtome (ESM-350, ERAM, Japan). There were total 12 samples, 3 for moisture testing and others for measurement. All slices were stored in distilled water for use.

Drying

Three slices were randomly selected as the MC test specimens. They were held together by a clip and put between a slide and a cover glass. No glue or any other fixing material was used. The same method was used for cell deformation observation specimens. All specimens were placed in a self-made sealed box and dried in a drying oven at 103 ± 2 °C.

Determination of MC

The mass of one slide glass, one cover glass, and two clips were determined before drying. The samples for cell deformation observation and the MC measuring were placed in the sealed box at 15 min intervals, and the real-time mass of specimens for MC measuring was recorded. The specimens for MC measuring were oven-dried and the moisture content M (%) at each stage of the drying process is calculated using Eq. 1 (Xue *et al*. 2018),

$$M = \frac{(Wn-w)-(W0-w)}{(W0-w)} \times 100(\%) \quad (1)$$

where W_n (mg) is the real-time mass of specimens at each stage of cell deformation, W_0 (mg) is the oven-dry mass, and w (mg) total mass of one slide glass, one cover glass, and two clips.

Observation of Specimens

The specimens from cell deformation were observed with an optical microscope (BX51, Olympus, Japan), and photographed in black and white using a microscopic digital camera (DP70, Olympus, Japan).

Image Processing and Analysis

The captured images were processed into binary images using the optimal threshold method (Fig. 1) with Adobe photoshop software (Adobe Systems Incorporated, San Jose, USA), and the binary images were converted into vector graphics by Adobe illustrator software. Two earlywood tracheids and two latewood tracheids in the intersection of wood ray and growth ring boundaries were randomly selected, and their centroids determined using Autodesk CAD (Autodesk, San Rafael, USA). An arbitrary quadrilateral ABCD (Fig. 2) was obtained by connecting the centroids. The area and circumference of the arbitrary quadrilateral ABCD and the radial and tangential lengths passing through the centroid of arbitrary quadrilateral ABCD were measured at 15 min intervals. The area and circumference shrinkage rates, and radial and tangential shrinkage rate of the arbitrary quadrilateral ABCD were calculated. The cell lumen area and radial and tangential length of earlywood and latewood tracheids adjacent to wood ray (blue area in Fig. 1(a2)), and in the middle of two wood rays (red area Fig. 1(a2)) were measured using Image Pro Plus software (Media Cybernetics, Rockville, USA). The area, radial and tangential shrinkage rates of tracheids were calculated.

The deformation of sapwood tracheids with the decrease of MC during the drying process, and the effect of wood ray on the deformation of the tracheid during the drying process were analyzed.

The area shrinkage rate, S_A (%), is calculated using Eq. 2,

$$S_A = \frac{(S_{An} - S_{A0})}{S_{A0}} \times 100(\%) \quad (2)$$

where S_{An} (μm^2) is the cell lumen area at each stage and S_{A0} (μm^2) is the initial cell lumen area.

The radial shrinkage rate, S_R (%), is calculated using Eq. 3,

$$S_R = \frac{(S_{Rn} - S_{R0})}{S_{R0}} \times 100(\%) \quad (3)$$

where S_{Rn} (μm) is the radial length at each stage and S_{R0} (μm) is the initial radial length.

The tangential shrinkage rate, S_T (%), is calculated using Eq. 4,

$$S_T = \frac{(S_{Tn} - S_{T0})}{S_{T0}} \times 100(\%) \quad (4)$$

where S_{Tn} (μm) is the tangential length at each stage and S_{T0} (μm) is the initial tangential length.

The circumference shrinkage rate, S_C (%), is calculated using Eq. 5,

$$S_C = \frac{(S_{Cn} - S_{C0})}{S_{C0}} \times 100(\%) \quad (5)$$

where S_{Cn} (μm) is the circumference of each stage and S_{C0} (μm) is the initial circumference.

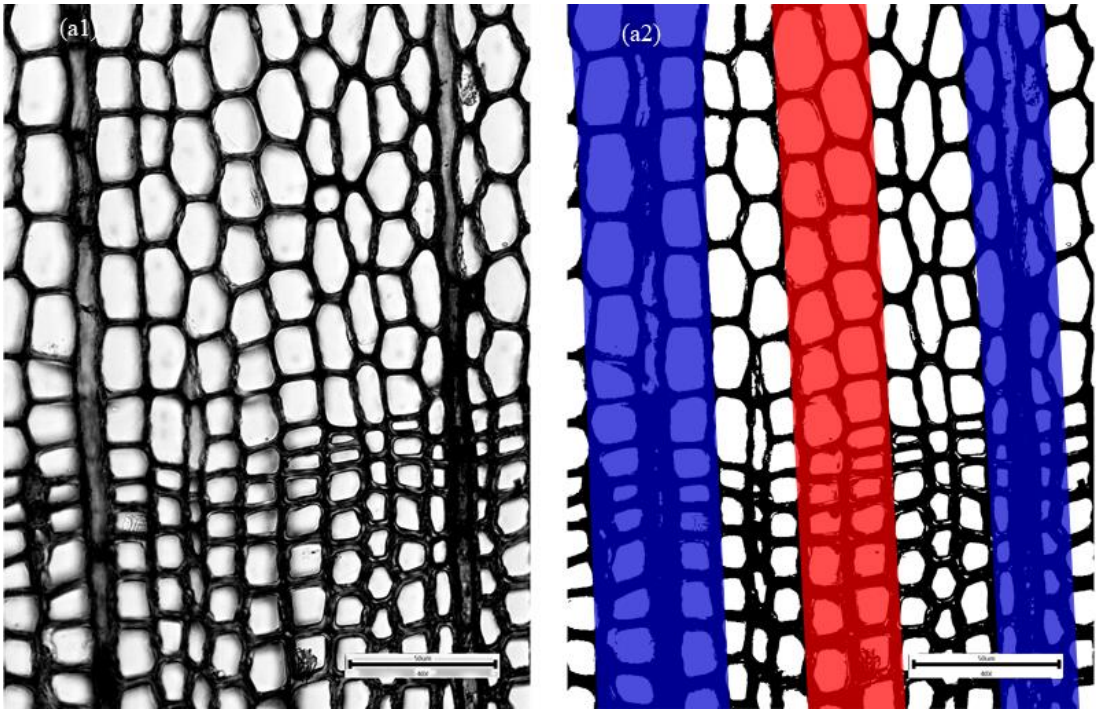

Fig. 1. The image processing method: a1: Original unprocessed image; and a2: binary image. The blue area highlights the cells closest to the wood rays; the red area indicate the cells between the wood rays.

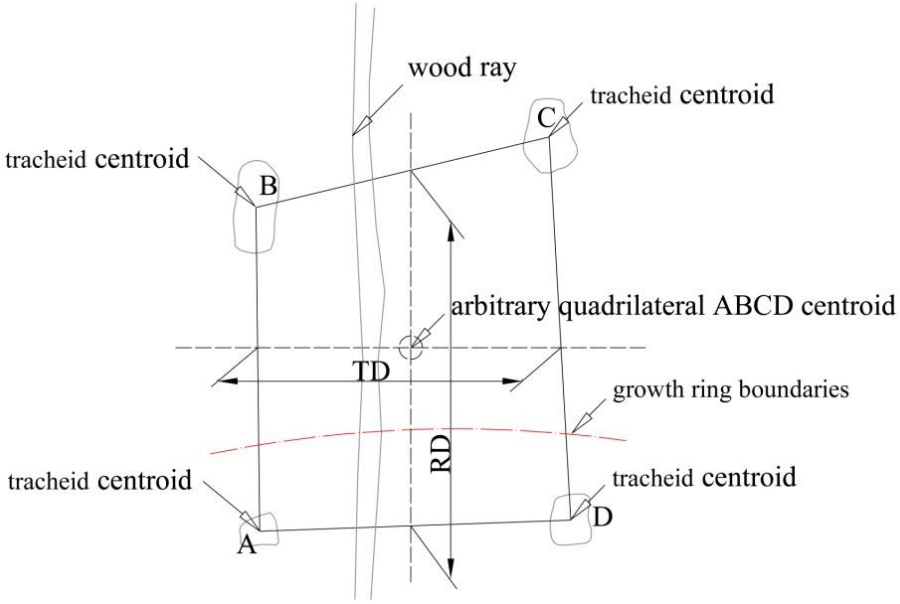

Fig. 2. The centroid measurement of arbitrary quadrilateral

RESULTS AND DISCUSSION

Change in MC and Microscopic Observation

The initial MC of the specimens was about 457.1%. The specimens were placed in a drying oven and removed at 15 min intervals. The MC decreased from 317.9% to 3.6% after a total of 11 observations. During the testing, the slices were directly taken out from the distilled water and placed on the slide glass. There was excess water, so the water content at the beginning stage showed a high value. Since visual observation is not an effective method to determine whether cell deformation occurred along with MC decrease, a binary transformation of the images was employed. This method enhanced the wave crest, wave trough, and improved the accuracy of the extracted features. However, the binary images obtained showed weak cell boundaries, and the cell wall of the *Taxodium* hybrid 'zhongshanshan' was too thin (Yu *et al*. 2007). Eventually, the latewood cells bound by growth rings were too difficult to distinguish in a clear and complete way. Therefore, this study only analyzed the cell lumen area of the *Taxodium* hybrid tracheids in order to determine the changes in cell area.

Arbitrary Quadrilateral Shrinkage

Figure 3 shows the change in regularity of the arbitrary quadrilateral ABCD. When the MC was above 100%, the area, radial, and tangential shrinkage rates of the arbitrary quadrilateral ABCD presented fluctuating changes with the decrease of MC and the change trend tended to be a horizontal straight line. When the MC was approximately 100% to 25%, the shrinkage of area, circumference and radial, and tangential length of the arbitrary quadrilateral ABCD showed a downward trend. The radial, tangential, and area shrinkage rates of the arbitrary quadrilateral ABCD was respectively 2.7%, 5.8%, and 8.1% when the MC of specimen was decreased to 3.57%, which is similar to the macroscopic shrinkage rate of one of its parental tree (*Taxodium distichum*) (FPL 2010).

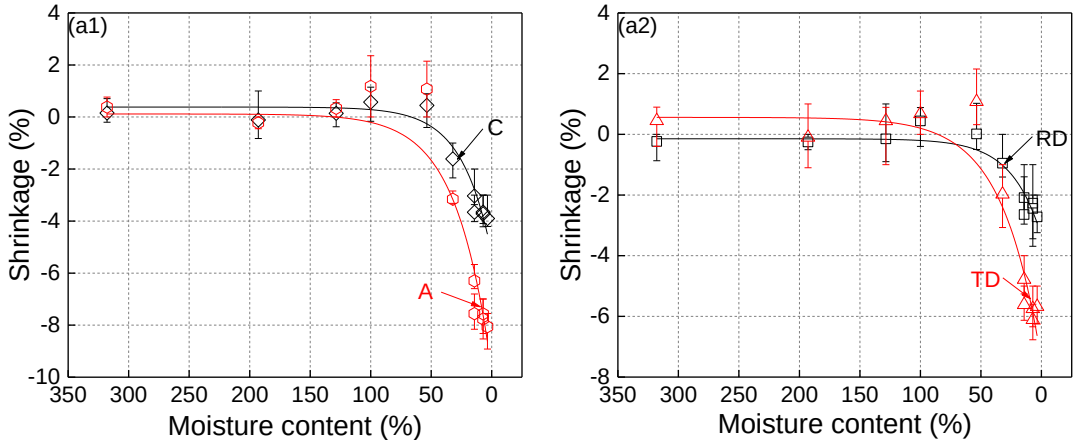

Fig. 3. Arbitrary quadrilateral shrinkage ABCD: A stands for the area of arbitrary quadrilateral; C stands for the circumference of arbitrary quadrilateral; RD denotes the radial direction; and TD stands for tangential direction. The shrinkage of area and circumference was plotted in (a1) and (a2), which describe the radial and tangential.

As shown in Fig. 3, when the MC was above 100%, the arbitrary quadrilateral deformation presented a fluctuating state, indicating shrinkage. During the drying process, the free water in the saturated wood cell lumen evaporated, leaving a concave meniscus in the pit membrane micropores, producing capillary tension. The latter has been shown to be inversely proportional to the curvature radius of the concave meniscus. The capillary tension acts on the whole cell wall by continuous free water, exerting an inward pulling force on the cell wall. As the water evaporates, the radius of curvature of the concave meniscus decreases. The maximum capillary tension was reached when the radius of curvature of the concave meniscus was the same as the radius of the pit membrane micropores. If the cell lumen was sealed during evaporation, then the capillary tension would be greater than the ultimate compressive strength parallel to the grain of wood, causing the shrinkage of wood cells. On the other hand, if the cell lumen contains air bubbles with a radius larger than the radius of curvature of the concave meniscus in the pit membrane micropores, the tension of concave meniscus formed at the gas-liquid interface of the bubble was smaller than the tension of concave meniscus formed in the pit membrane micropores. In this case, the bubbles expand to offset the inward pulling force applied on partial cell wall, and fluctuating deformation of cell shape occurred (Wentzel-Vietheer *et al*. 2013). As can be seen in Fig. 3, the wood shrinkage happened when the MC was close to 50%. This is linked to the very structure of the cell, with its primary and secondary wall, and the intercellular layer. The bound water is located in the primary and secondary wall, and the free water is located in the intercellular layer. The free water in the intercellular layer begins to evaporate when the MC of wood is above the FSP and leads to shrinkage (Liu and Zhao 2012).

Tracheid Shrinkage

Figure 4 shows the change regularity of the cell lumen area, and the radial and tangential lengths of earlywood and latewood tracheids in the *Taxodium* hybrid 'zhongshanshan'. The tangential shrinkage of the tracheids was larger than their radial shrinkage, and the latewood showed greater radial and tangential shrinkage than earlywood. Figure 4(a1) shows how, an enlarged cell lumen of latewood tracheids when the MC was approximately between 100% to 25%. This could be due to the smaller size of

the tracheids in latewood, causing the free water in the cell lumen to evaporate first. Only when the MC decreased to 100%, and the free water in the cell lumen evaporated completely did the bound water in the cell wall and the free water in the intercellular layer began to evaporate. The other tracheids formed a relatively stable shape due to capillary tension, ultimate compressive strength parallel to the grain, and the expansion of air bubbles in the cell lumen, resulting in enlargement of the latter in latewood tracheids. As the MC continued to decrease below 25%, the free water in the wood evaporated completely, and all tracheids shrunk normally.

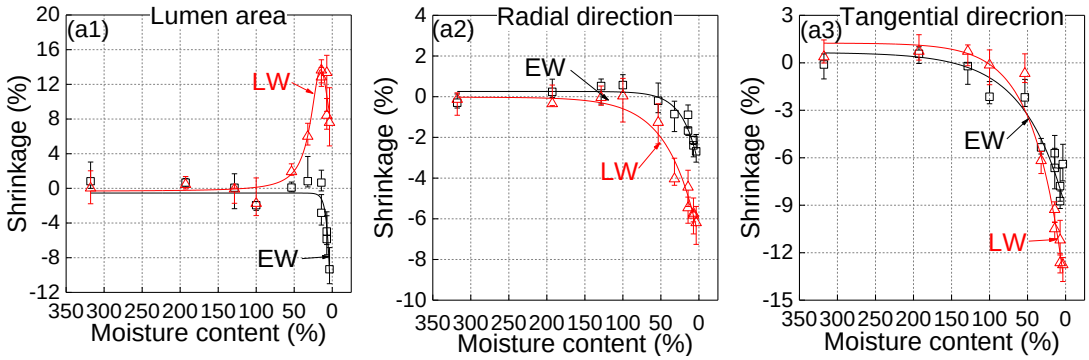

Fig. 4. Tracheid shrinkage: EW stands for earlywood; LW indicates latewood. The shrinkage of lumen area is plotted in (a1), while (a2) shows the tracheid radial direction shrinkage, and (a3) describes the tangential shrinkage.

As shown in Fig. 4(a2), the latewood began to shrink in the radial direction when the MC was about 100%, while the earlywood began to shrink in the radial direction when the MC was nearly 50%. Figure 4(a3) confirms that earlywood and latewood tracheids exhibited synchronous tangential shrinkages. Smaller latewood tracheids take the lead in evaporating the bound water of cell wall and the free water of intercellular layer, and thus latewood tracheids shrink first (Chauhan and Aggarwal 2004). Radial shrinking times differ, as earlywood and latewood do not affect each other. In the tangential direction, the shrinkage of the earlywood and latewood is synchronous because the shrinkage of the latewood drives the earlywood to shrink together.

The Effect of Wood Ray on the Tracheid Shrinkage

Figure 5 shows the change in regularity of the cell lumen area and radial and tangential lengths of *Taxodium* hybrid 'zhongshanshan' tracheids on both sides and in the middle of the wood ray with decreasing MC. Overall, the wood ray had little effect on the cell lumen and tangential shrinkages of the tracheids. The tracheids on both sides of the wood ray exhibited less radial shrinkage than tracheids between the wood rays. These results were consistent with the theory of 'radiation restraint' at the micro-scale, indicating that the wood rays have a certain effect on the radial shrinkage of the tracheids.

The wood ray did not affect the change in regularity of the tracheid cell lumen (Figs. 5(a1) and 5(a2)). For latewood tracheids located on both sides of the wood ray, when the MC was 100% to 25%, the smaller tracheids presented obviously enlarged cell lumens. The cell lumen of larger tracheids was almost unaffected by the wood ray (Fig. 5(a2)). The radial shrinkage of the earlywood tracheids on both sides of the wood ray was as much as half of the radial shrinkage of the tracheids between the wood ray (Fig. 5 (b1)). The wood ray has a greater effect on radial shrinkage of latewood tracheids (Fig. 5(b2)).

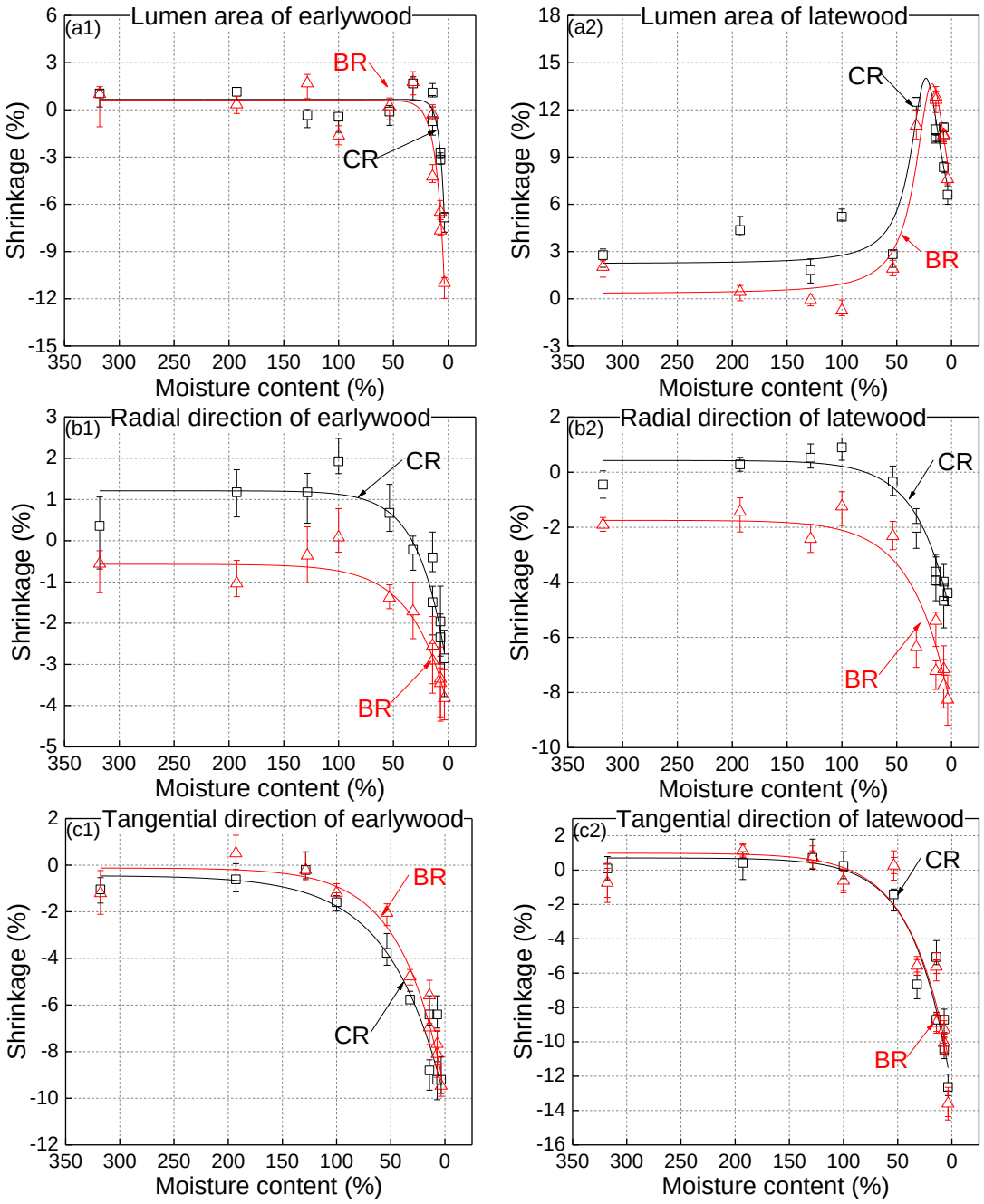

Fig. 5. The effect of wood rays on tracheid shrinkage: CR indicates a tracheid close to the wood ray; BR indicates a tracheid between two wood rays; (a1, a2) denote the shrinkage behavior of latewood and earlywood tracheids lumen area plots; (b1, b2) show tracheid radial shrinkages; and (c1, c2) describe latewood and earlywood tracheid tangential shrinkages.

The wood ray cells are arranged perpendicular to the tracheids. As the wood ray cells shrunk, the longitudinal shrinkage was smaller than the transverse shrinkage; thus the radial shrinkage of the tracheids on both sides of the wood ray was suppressed. However, the wood ray's inhibitory effect was only observed on tracheids adjacent to it. Therefore, the radial shrinkage of the tracheids between the two wood rays appeared to show a 'small to large to small' trend (Xue *et al*. 2018). The wood ray had little effect on the tangential

shrinkage of the tracheids (Figs. 5(c1) and 5(c2)). When the MC was close to 50%, the earlywood tracheids on both sides of the wood ray showed slightly larger tangential shrinkage than earlywood tracheids between the wood rays. A possible explanation is that the difference of cell wall thickness and cell lumen size between earlywood and latewood tracheids has an effect on how much influence the wood ray has on the evaporation of free water.

Fiber Saturation Point (FSP)

The relationship between shrinkage and MC can be analyzed mathematically using a curve-fitting modeling method to determine the FSP (Babiak and Kúdela 1995). The MC and the area, circumference, and radial and tangential shrinkage rates of the arbitrary quadrilateral ABCD showed a downward trend, and there was no obvious inflection point in the portion where the shrinkage rate changed from sharply and slowly. The downward trend, and the empirical formula obtained by cubic polynomial fitting indicated a good polynomial curve fit between the shrinkage rate and the MC, as shown in Table 1.

Table 1. Empirical Formula for Fitting Shrinkage Rate and MC of Arbitrary Quadrilateral ABCD

Values	Fitting Formulas	R^2
Area of arbitrary quadrilateral ABCD	$y = -0.00004x^3+0.0046x^2+0.0493x-8.3062$	0.9925
Circumference of arbitrary quadrilateral ABCD	$y = -0.00002x^3+0.0022x^2+0.0211x-3.9866$	0.9921
Radial direction of arbitrary quadrilateral ABCD	$y = -0.000009x^3+0.0009x^2+0.0293x-2.7617$	0.9563
Tangential direction of arbitrary quadrilateral ABCD	$y = -0.00003x^3+0.0033x^2+0.0323x-6.1962$	0.9884

At FSP, the value of x in the MC range (3.57% to 100%), the shrinkage rate would increase correspondingly with increasing MC at (3.57, x). At (x, 100), the shrinkage rate showed slight changes along with the MC. By studying the properties of the fitted curve, the inflection point of the curve growth at this interval was the FSP (Guan *et al*. 2003).

By deriving the fitting equation of the area shrinkage of arbitrary quadrilateral ABCD, following equations were obtained:

$$y' = -0.00012x^2 + 0.0092x + 0.0493 \quad (6)$$

$$y'' = -0.00024x + 0.0092 \quad (7)$$

The calculated x = 38.3, indicates that the inflection point of the curve was at (3.57, 38.3). When x = 38.3, the above equations reached the maximum value at (3.57, 100), indicating that the shrinkage rate of the *Taxodium* hybrid 'zhongshanshan' increased with increasing MC and reached the maximum value when the MC reached 38.3%. As the MC continued to increase, the increase in shrinkage rate was slowed down. Based on the area shrinkage rate of quadrilateral ABCD, the FSP of the *Taxodium* hybrid 'zhongshanshan' was obtained (FSP_A = 38.33%).

Similarly, each FSP was obtained based on the relationship between the circumference, radial and tangential shrinkage rates, and the MC of arbitrary quadrilateral ABCD. In summary, the FSP of the *Taxodium* hybrid 'zhongshanshan' was between 33.33% and 38.33%.

Table 2. Fiber Saturation Points Obtained by Relating Shrinkage Rate and MC

Values	Fitting Formulas	FSP
Circumference of arbitrary quadrilateral ABCD	$y' = -0.00006x^2 + 0.0044x + 0.0211$ $y'' = -0.00012x + 0.0044$	36.67
Radial direction of arbitrary quadrilateral ABCD	$y' = -0.000027x^2 + 0.0018x + 0.0293$ $y'' = -0.000054x + 0.0018$	33.33
Tangential direction of arbitrary quadrilateral ABCD	$y' = -0.0009x^2 + 0.0066x + 0.0323$ $y'' = -0.00018x + 0.0066$	36.67

CONCLUSIONS

1. In this study, the arbitrary quadrilateral ABCD structure was used to characterize the deformation of the *Taxodium* hybrid 'zhongshanshan' at a microscale level. The radial and tangential shrinkage rates obtained were 2.7% and 5.8%, respectively. This was similar to the macroscopic shrinkage of the parental *Taxodium distichum*. Microscopic and macroscopic deformations were consistent with each other.
2. According to the analysis of the data, when the moisture content (MC) was above the FSP, the wood cells also shrank, and the wood cell exhibited a shrink-swell cycle pattern as the MC decreased.
3. When the MC of the latewood tracheid was reduced to 100%, the cell lumen was greatly enlarged.
4. The tangential shrinkage of the *Taxodium* hybrid 'zhongshanshan' tracheid was greater than its radial shrinkage, and the radial and tangential shrinkages of latewood tracheids was larger than earlywood.
5. Wood ray had little effect on the cell lumen and tangential shrinkage, and had a great influence on the radial shrinkage of tracheids adjacent to the wood ray. The shrinkage anisotropy of the *Taxodium* hybrid 'zhongshanshan' was the result of combined effect of the difference between earlywood and latewood, and the inhibitory effect of the wood ray.
6. The FSP of *Taxodium* hybrid 'zhongshanshan' was between 33.3% and 38.3%.

ACKNOWLEDGEMENTS

This research was supported by the Jiang Su Agricultural Science and Technology Innovation Fund (Grant no. CX(16)1005) and by the Plant Germplasm Resources Innovation Project of Strategic Bioresources Service network of Chinese Academy of Sciences (grant no. ZSZC-009). The financial support received from these projects is gratefully acknowledged.

REFERENCES CITED

Babiak, M., and Kúdela, J. (1995). "A contribution to the definition of the fiber saturation point," *Wood Science and Technology* 29(3), 217-226. DOI: 10.1007/BF00204589

Bonarski, J. T., Kifetew, G., and Olek, W. (2015). "Effects of cell wall ultrastructure on the transverse shrinkage anisotropy of Scots pine wood," *Holzforschung* 69(4), 501-507. DOI: 10.1515/hf-2014-0075

Chauhan, S. S., and Aggarwal, P. (2004). "Effect of moisture sorption state on transverse dimensional changes in wood," *Holz als Roh- und Werkstoff* 62(1), 50-55. DOI: 10.1007/s00107-003-0437-y

Dang, D., Moutou, P. R., Toussaint E., and Grédiac, M. (2018). "Inverse identification of early- and latewood hydric properties using full-field measurements," *Wood Material Science and Engineering* 13(1), 50-63. DOI: 10.1080/17480272.2016.1263973

Forest Products Laboratory (FPL) (2010). "Mechanical properties of wood," in: *Wood Handbook, Wood as an Engineering Material*, U. S. Department of Agriculture, Madison, WI, USA.

Gu, H., Zink-Sharp, A., and Sell, J. (2001). "Hypothesis on the role of cell wall structure in differential transverse shrinkage of wood," *Holz als Roh- und Werkstoff* 59(6), 436-442. DOI: 10.1007/s001070100240

Guan, M. J., Zhu, Y. X., and Zhang, Q. S., (2003). "Research on FSP of *Dendrocalamus membranaceus* according to its shrinkage," *Journal of Bamboo Research* 22(3), 40-43 (in Chinese).

Hua, J. F., Han, L. W., Gu, C. S., and Yin, Y. L., (2017). "Morpho-anatomical and photosynthetic responses of *Taxodium* hybrid 'zhongshanshan' 406 to prolonged flooding," *Flora* 231(6), 29-37. DOI: 10.1016/j.flora.2017.04.007

Liu, Y. X., and Zhao, G. J. (2012). "Wood cells," in: *Wood Science*, China Forestry Publishing House, Beijing.

Murata, K., and Masuda, M. (2006). "Microscopic observation of transverse swelling of latewood tracheid: effect of macroscopic/mesoscopic structure," *Journal of Wood Science* 52(4), 283-289. DOI: 10.1007/s10086-005-0760-5

Pambou Nziengui, C. F., Ikogou, S., and Moutou Pitti, R. (2017). "Impact of cyclic compressive loading and moisture content on the mechanical behavior of *Aucoumea klaineana* Pierre," *Wood Material Science and Engineering* 13(4), 190-196. DOI: 10.1080/17480272.2017.1307281

Panshin, A. J., and Zeeuw, C. D. (1980). "Structure," in: *Textbook of Wood Technology*, McGraw-Hill, New York.

Shi, Q., Yin, Y. L., Wang, Z. Q., Fan, W. C., and Hua, J. F. (2016). "Physiological acclimation of *Taxodium* hybrid 'Zhongshanshan 118' plants to short-term drought stress and recovery," *HortScience* 51(9), 1159-1166. DOI: 10.21273/HORTSCI10997-16

Spear, M., and Walker, J. (2006). "Dimensional instability in timber," in: *Primary Wood Processing, Principles and Practice*, Springer, Berlin.

Taguchi, A., Murata, K., and Nakano, T. (2010). "Observation of cell shapes in wood cross-sections during water adsorption by confocal laser-scanning microscopy (CLSM)," *Holzforschung* 64(5), 627-631. DOI: 10.1515/hf.2010.092

Taylor, A., Plank, B., Standfest, G., and Petutschnigg, A. (2013). "Beech wood shrinkage observed at the microscale by a time series of X-ray computed tomographs

(μXCT)," *Holzforschung* 67(2), 201-205. DOI: 10.1515/hf-2012-0100

Thuvander, F., Kifetew, G., and Berglund, L. A. (2002). "Modeling of cell wall drying stresses in wood," *Wood Science and Technol*ogy 36(3), 241-254. DOI: 10.1007/s00226-001-0134-0

Wentzel-Vietheer, M., Washusen, R., Downes, G. M., Harwood, C., Ebdon, N., and Ozarska, B. (2013). "Prediction of non-recoverable collapse in *Eucalyptus globulus* from near infrared scanning of radial wood samples," *European Journal of Wood and Wood Products* 71(6), 755-768. DOI: 10.1007/s00107-013-0735-y

Xue, Q. W., Sun, W. H., Fagerstedt, K., Guo, X., Dong, M. R., Wang, W. B., and Cao, H. M. (2018). "Effects of wood rays on the shrinkage of wood during the drying process," *BioResources* 13(3), 7086-7095. DOI: 10.15376/biores.13.3.7086-7095

Yu, H. Q., Fei, B. H., Zhao, R. J., Liu, J. L., and Zhang, X. Y. (2007). "Anatomical characteristics of *Taxodium* 'zhongshansa302' and *Taxodium distichum* wood," *Forest Research* 20(2), 213-217 (in Chinese).

Article submitted: April 11, 2019; Peer review completed: June 3, 2019; Revised version received: June 10, 2019; Accepted: June 14, 2019; Published: June 19, 2019.
DOI: 10.15376/biores.14.3.6219-6230